Electronic phase separation at $LaAlO_3/SrTiO_3$ interfaces tunable by oxygen deficiency

V. N. Strocov,[1] A. Chikina,[1] M. Caputo,[1] M.-A. Husanu,[1,2] F. Bisti,[1] D. Bracher,[1] T. Schmitt,[1] F. Miletto Granozio,[3] C. A. F. Vaz,[1] and F. Lechermann[4]

[1]*Swiss Light Source, Paul Scherrer Institute, CH-5232 Villigen-PSI, Switzerland*

[2]*National Institute of Materials Physics, Atomistilor 405A, RO-077125 Magurele, Romania*

[3]*CNR-SPIN, Complesso universitario di Monte S. Angelo, Via Cintia, I-80126 Naples, Italy*

[4]*Institut für Theoretische Physik, Universität Hamburg, Jungiusstr. 9, DE-20355 Hamburg, Germany*

(Received 12 June 2019; published 7 October 2019)

Electronic phase separation is crucial for the fascinating macroscopic properties of the $LaAlO_3/SrTiO_3$ (LAO/STO) paradigm oxide interface, including the coexistence of superconductivity and ferromagnetism. We investigate this phenomenon using angle-resolved photoelectron spectroscopy (ARPES) in the soft-x-ray energy range, where the enhanced probing depth combined with resonant photoexcitation allow us access to fundamental electronic structure characteristics – momentum-resolved spectral function, dispersions and ordering of energy bands, Fermi surface – of buried interfaces. Our experiment uses x-ray irradiation of the LAO/STO interface to tune its oxygen deficiency, building up a dichotomic system where mobile weakly correlated Ti t_{2g} electrons coexist with localized strongly correlated Ti e_g ones. The ARPES spectra dynamics under x-ray irradiation shows a gradual intensity increase under constant Luttinger count of the Fermi surface. This fact identifies electronic phase separation (EPS) where the mobile electrons accumulate in conducting puddles with fixed electronic structure embedded in an insulating host phase, and allows us to estimate the lateral fraction of these puddles. We discuss the physics of EPS invoking a theoretical picture of oxygen-vacancy clustering, promoted by the magnetism of the localized Ti e_g electrons, and repelling of the mobile t_{2g} electrons from these clusters. Our results on the irradiation-tuned EPS elucidate the intrinsic one taking place at the stoichiometric LAO/STO interfaces.

DOI: 10.1103/PhysRevMaterials.3.106001

I. INTRODUCTION

An inherent feature of many transition metal oxides (TMOs) is electronic phase separation (EPS), which is the spontaneous formation on the micro- to nanoscale of regions possessing different electronic and magnetic properties. This phenomenon is crucial, for example, for colossal magnetoresistance in manganites and the stripe order in cuprates [1–3]. The EPS phenomenon naturally propagates to interfaces of the TMOs. For the $LaAlO_3/SrTiO_3$ (LAO/STO) interface, the "drosophila" of oxide electronics where a mobile electron system (MES) is spontaneously formed – for entries see the reviews [4,5] – the EPS can be particularly strong because the huge dielectric constant of the nearly ferroelectric STO largely screens the electron repulsion and thus allows coagulation of large electron densities [6]. The EPS has been identified, for example, in a percolative metal-to-superconductor transition where a significant fraction of MES resists condensation to the superconducting ground state down to the lowest temperature [7,8]. On the magnetic side, ferromagnetic (FM) puddles embedded in the metallic superconducting phase, observed in magnetotransport [9], magnetic torque magnetometry [10], and the superconducting quantum interference device (SQUID) [11] experiments, explain the intriguing coexistence of the ferromagnetic and superconductive properties of the LAO/STO interface. Magnetoresistance, anomalous Hall effect, and tunneling experiments [8,12,13] have also evidenced the presence of EPS at this interface. This phenomenon is extremely important from a device perspective [14] explaining why the interfacial charge carrier concentration n_s observed in transport properties of the LAO/STO interface always falls short of the predictions of the mean-field theories. Furthermore, the EPS can be tuned by an external electric field [6,15]. An angle-resolved photoelectron spectroscopy (ARPES) study of the EPS with the coexistence of metallic and insulating phases on bare STO(100) and (111) surfaces has been reported by Dudy *et al.* [16].

Oxygen vacancies (V_Os) dramatically affect electronic and magnetic properties of all TMO systems. In a simplified picture of oxygen-deficient (OD) LAO/STO interfaces, each V_O on the STO side releases two electrons. One fraction of them joins the MES formed by delocalized quasiparticles, which are Ti t_{2g} derived, weakly correlated, nonmagnetic and split by Rashba spin-orbit interaction [17], and form large polarons [18,19]. Sufficiently high concentrations of V_Os result in a dimensionality transformation of the MES from two-dimensional (2D) to quasi-three-dimensional (quasi-3D) [20–22]. Another fraction of electrons released by the V_O stays near the Ti ion to form there a localized in-gap state (IGS) at binding energy $E_B \sim -1.3$ eV, which is Ti e_g derived, strongly correlated, magnetic, and is often viewed as a small polaron. These states determine the interfacial ferromagnetism of OD-LAO/STO [23,24]. This theoretical picture of the dichotomic electron system formed at the OD-LAO/STO interface [25–28] has recently been experimentally confirmed by resonant photoemission (ResPE) experiments [29]. The coexistence of the two radically different MES and IGS electron subsystems much enriches the physics of

the OD-LAO/STO interfaces compared to the stoichiometric ones. As we will see below, the V_Os can also be used as a knob to tune the EPS, making the OD-LAO/STO interfaces the ideal platform to study this phenomenon.

Here, we demonstrate controllable tuning of the EPS at the OD-LAO/STO interfaces by generation of V_Os with intense soft x rays from a synchrotron source. The electronic structure in this system is monitored by soft-x-ray ARPES (SX-ARPES), leveraging its enhanced probing depth and chemical specificity achieved by resonant photoexcitation. Following the evolution of the **k**-resolved electron dispersions and Fermi surface of the MES as a function of x-ray irradiation dose, we identify the EPS and estimate the lateral MES fraction developing with increase of the V_O concentration. Finally, we elucidate a theoretical model of the EPS, which finds a clustering tendency of the V_Os and repulsion of the MES electrons from these clusters.

II. SAMPLE PREPARATION AND SX-ARPES EXPERIMENT

OD-LAO/STO samples are a convenient platform to study the EPS. We have grown such samples on TiO_2-terminated STO(100) using pulsed laser deposition (PLD). Before the LAO growth, the substrates were annealed in vacuum at 500 °C for 30–40 min till the appearance of the characteristic reflection high-energy electron diffraction (RHEED) pattern. Then a 4 u.c. thick layer of LAO was deposited at 800 °C in O_2 pressure reduced to 8×10^{-5} mbar. Whereas in the standard protocols [30] the growth is immediately followed by in situ annealing in O_2 at 500 °C, we cooled down the as-grown samples, and then postannealed them ex situ in O_2 at the same temperature for about 24 h to ensure their complete saturation by oxygen [29].

Our **k**-resolved SX-ARPES experiments – for a recent review of this technique and its spectroscopic advantages see Ref. [31] – used resonant photoexcitation at the Ti L edge that boosted photoemission response of the Ti-derived electron states at the buried interface. The measurements were performed at the SX-ARPES endstation [32] of the Advanced Resonant Spectroscopies (ADRESS) beamline [33] of the Swiss Light Source, Paul Scherrer Institute, Switzerland. The photon flux was around 10^{13} photons/s and focused into a spot of 30×75 μm^2 on the sample surface at an x-ray grazing incidence angle of 15°. The x-ray absorption spectroscopy (XAS) data were measured in the total electron yield (TEY) mode. For the ARPES measurements, the combined (beamline and analyzer) energy resolution was set to ~50 meV. The sample temperature was kept at 12 K in order to suppress smearing of the coherent spectral structure [34] as well as allow buildup of the V_Os. The series of Ti $2p$ core-level spectra depending on irradiation time (t_{irr}) were measured in intervals of 90 s, and ResPE spectra in intervals of 25 s. All series were averaged over five different points on the sample starting from fresh spots. Photoemission electron microscopy (PEEM) experiments aiming at spatial resolution of the nucleation and clustering of the V_Os (Supplemental Material 4 [35]) were carried out at the Surface and Interface Microscopy (SIM) beamline [36] of the Swiss Light Source.

V_Os on the STO side of the LAO/STO interfaces are readily identified by their characteristic signatures in the photoemission spectra, the IGS peak in the valence band (VB) and Ti^{3+} component in the Ti $2p$ core level spectra [19,29]. SX-ARPES characterization of our fresh samples did not detect these spectral structures. This evidences that the postannealing quenched the V_Os in our samples below the sensitivity of our photoemission experiment of the order of 1%. It has been reported, however, that postannealed samples deviate from the ST ones on their transport properties [30]. We will see below that this deviation traces back not only to n_s but also to nanoscale properties of the MES. Importantly, our samples appear susceptible to x-ray irradiation: Whereas the ST samples are practically immune to it [18], ours, presumably due to nonperfect recovery of their crystallinity from the oxygen-deficient postgrowth state, under x-ray irradiation were readily losing oxygen to form V_Os in STO, as evidenced by the buildup of the IGS and Ti^{3+} signals. Such a dependence of the sample properties on the growth and annealing protocol goes along with the known sensitivity of STO substrates to their history with respect to the environmental conditions and temperature [37]. In particular, we have found that the rate of V_O generation by x-rays strongly increases with the STO substrate temperature during its pregrowth annealing in vacuum, when V_Os might preform near its surface, and on O_2 pressure during the deposition of LAO. Interestingly, an increase of sample temperature above ~120 K, as well as x-ray irradiation of samples in O_2 pressure of about 10^{-7} mbar, quench the x-ray generated V_Os. This can possibly be explained by the fact that x-ray irradiation cracks the physisorbed O_2 molecules into atomic oxygen [16,38], which can effectively penetrate into the LAO/STO heterostructure to quench the V_Os.

Secondary ion mass spectrometry analysis of O^{16} to O^{18} isotope substitution under x-ray irradiation, reported elsewhere [22], suggests that the x-ray generated V_Os do not propagate beyond the top TiO_2 layer of STO. We note that the x-ray induced creation of the V_O in STO implies efficient out-diffusion of oxygen through the LAO layer. Although well-established down to room temperature [39], this process should however totally freeze at the sample temperature ~12 K during our SX-ARPES experiments, where kT is three orders of magnitude smaller than the activation energy of V_Os. Such an oddity is highly nontrivial and may suggest nonconventional oxygen migration mechanisms [22].

III. OVERVIEW OF THE ELECTRONIC STRUCTURE OF OD-LAO/STO INTERFACES

The electronic structure of the Ti-derived IGS and MES subsystems at the STO side of the OD-LAO/STO interface can be explored by ResPE at the Ti L edge [19,40,41]. Figure 1(a) shows the experimental ResPE intensity as a function of E_B and excitation energy ($h\nu$) measured after an x-ray irradiation for about 2 h. Above the broad VB composed by the O $2p$ states in STO and LAO, the map shows the hallmark of the V_Os, the broad resonating peak at $E_B \sim -1.3$ eV identifying the e_g-derived IGSs. The narrow resonating peak at E_F identifies the t_{2g}-derived MES. For a detailed analysis of the ResPE behavior of OD-LAO/STO see Ref. [29].

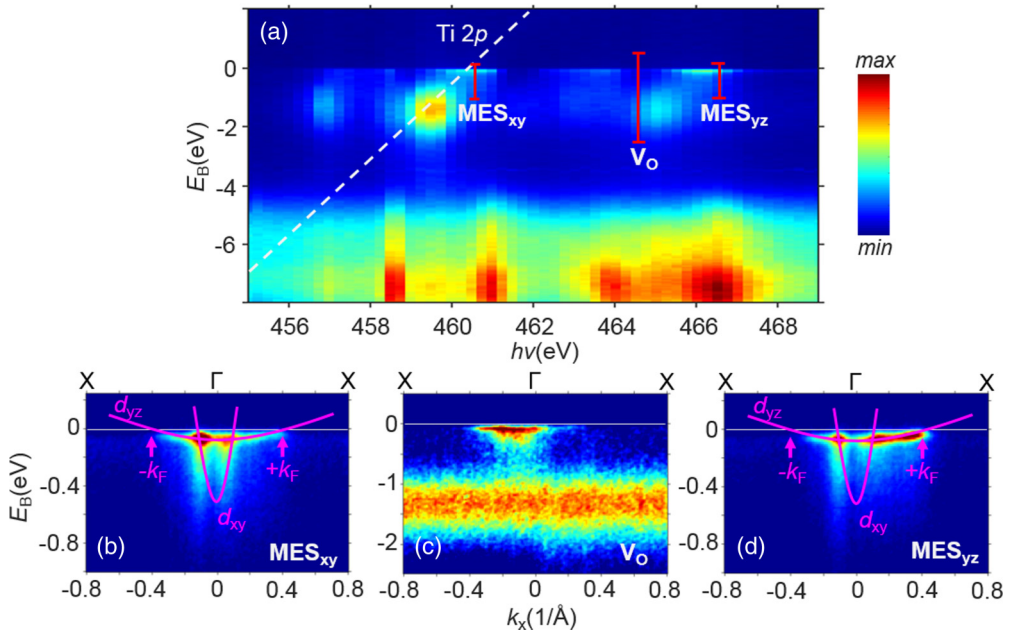

FIG. 1. ResPE of OD-LAO/STO: (a) angle-integrated ResPE intensity through the L_3 and L_2 edges. The IGS-peak at $E_B \sim -1.3$ eV signals the V_Os; (b)–(d) ARPES intensity images measured at $h\nu = 460.4$, 464.4, and 466.4 eV, which enhance, respectively, the MES-d_{xy} states, V_O-induced IGS, and MES-d_{yz} states. These $h\nu$ values and corresponding E_B intervals of the images marked in red on (a). The d_{xy} and d_{yz} dispersions are sketched.

The ARPES intensity images, taken at the $h\nu$ values marked at the above ResPE map, are shown in Figs. 1(b)–1(d). Measured with *s*-polarized incident x-rays, these images reflect the antisymmetric d_{xy} and d_{yz} bands sketched on top [18,42] as well as the disordered IGSs. The d_{xy} band, due to its narrow interfacial localization, loses its photoexcitation cross-section at high energies [43] but is manifested by two bright points where it hybridizes with the d_{yz} band due to the symmetry breaking caused by lattice distortions [18] as well as spin-orbit interaction [17]. The image 1(b) is taken at the Ti L_3 edge, where the d_{xy} to d_{yz} intensity ratio is higher compared to the L_2 edge [29], at $h\nu = 460.4$ eV delivering sufficient separation of the MES peak from the Ti $2p$ core-level one excited by second-order x-ray radiation. Fig. 1(c) is characteristic of the broad dispersionless IGSs. It is taken at the L_2 edge (at the L_3 edge the IGSs overlap with the Ti $2p$ stray intensity) at $h\nu = 464.4$ eV, where the IGS signal resonantly scales up and the MES one scales down. The image in Fig. 1(d) measured at $h\nu = 466.4$ eV is characteristic of the d_{yz} band, whose intensity ratio to the d_{xy} one enhances compared to the L_2 edge. To highlight the predominant spectral contribution, the images in Figs. 1(c)–1(e) and the corresponding $h\nu$ values on the ResPE map are marked as MES$_{xy}$, V_O, and MES$_{yz}$.

The band order and band dispersions observed in OD-LAO/STO adopt the same pattern as in ST-LAO/STO [18,42]. The band filling in OD-LAO/STO is somewhat larger, however, as characterized by the Fermi momentum k_F of the d_{yz} band in Fig. 1(d) increasing to $\sim 0.4\,\text{Å}^{-1}$ compared to $\sim 0.33\,\text{Å}^{-1}$ for ST-LAO/STO [18,42]. Furthermore, the weight of the polaronic hump and thus renormalization of the effective mass m^* reduce to ~ 1.5 compared to ~ 2.5 in ST-LAO/STO [18]. Importantly, although the V_Os generated by x-rays in STO are located predominantly in its top TiO_2 layer, analysis of out-of-plane ARPES dispersions [22] evidences that the resulting MES has actually quasi-3D character, with its penetrating depth into STO being more than 30 Å [21]. The large spatial extension of electron states generated by the localized V_Os is similar to the doping of conventional semiconductors with a tiny amount of foreign atoms.

IV. ELECTRONIC PHASE SEPARATION

A. X-ray irradiation dynamics

The effect of x-ray irradiation on the electronic structure of our OD-LAO/STO samples is illustrated in Fig. 2 by (downsampled) series of t_{irr}-dependent angle-integrated photoemission spectra collected in different spectral regions. Fig. 2(a) shows the Ti $2p$ core-level spectra measured at $h\nu = 1000$ eV. The increase of their Ti^{3+} component manifests the buildup of V_Os which reduces the Ti^{4+} ions to the 3^+ valency. The apparent Ti^{3+} to Ti^{4+} spectral weight ratio reaches ~ 0.1 at maximal t_{irr}. Taking into account the location of V_Os in predominantly in the top STO layer [22] and a photoelectron mean-free-path λ of ~ 11 Å at our kinetic energy [38,44], this figure indicates that about 30% of the Ti ions in this layer become Ti^{3+}. Panels (b) and (c) show t_{irr}-dependent angle-integrated ResPE spectra of the VB integrated through the first Brillouin zone. The series in Fig. 2(b) was measured at $h\nu = 464.4$ eV, which boosts the IGS peak at $E_B \sim -1.3$ eV, see Fig. 1(a). Negligible at the zero-t_{irr} limit, its intensity and thus IGS concentration gradually increases under irradiation. Figures 2(c) and 2(d) show development of the MES signal at $h\nu = 460.4$ and 466.4 eV marked as MES$_{xy}$ and MES$_{yz}$,

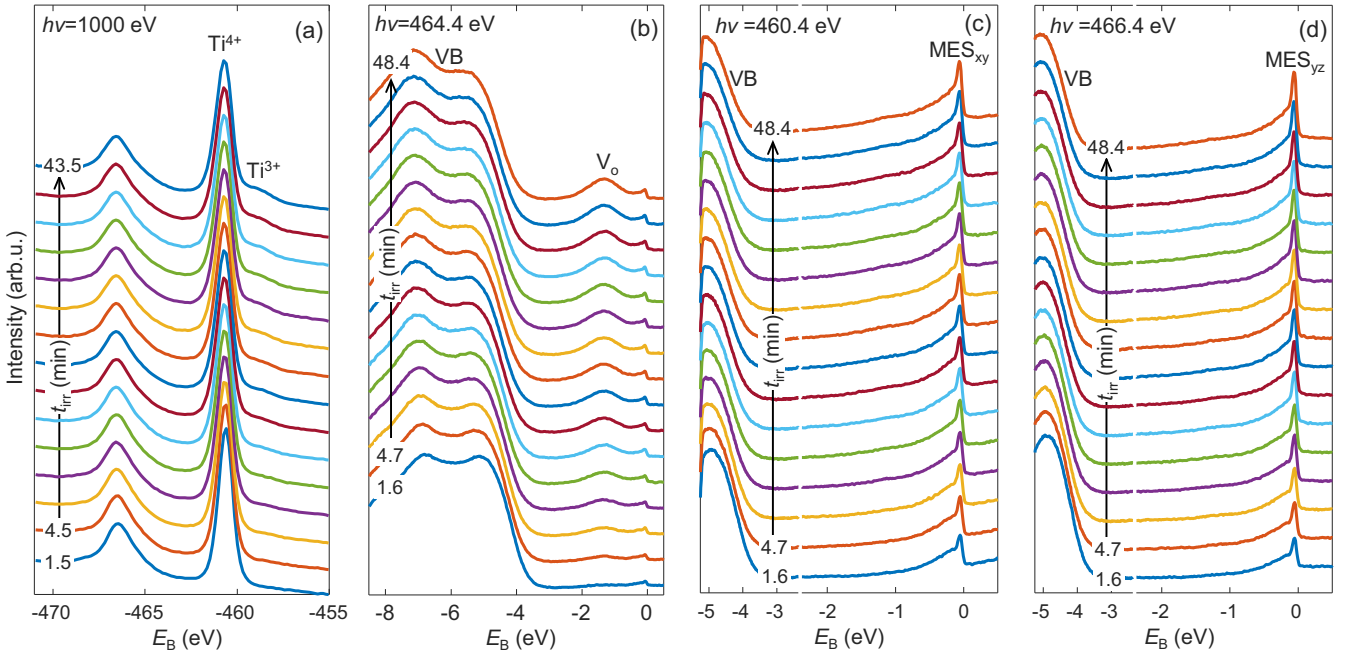

FIG. 2. x-ray irradiation effect on electronic structure of the OD-LAO/STO interface: (a) Ti $2p$ core-level spectra, where the Ti^{3+} component corresponds to the V_Os; ResPE spectra measured (b) through the whole VB at $h\nu = 464.4$ eV boosting the IGS peak, and (c)–(d) at $h\nu = 460.4$ and 466.4 eV boosting response of the d_{xy} and d_{yz} states, respectively. Note the different energy scale of the VB vs V_o and MES regions in (c) and (d). The experimental series are down sampled to the indicated time intervals. Under x-ray irradiation the Ti^{3+} core level, IGS and MES intensity increase, following buildup of the V_Os.

respectively, to highlight the predominant spectral contribution. The increase of this signal with t_{irr} manifests the increase of the integral MES concentration, following the V_O buildup. The observed evolution of both IGS and MES peaks reflects the fact that the V_Os inject localized electrons into the IGSs and mobile ones into the MES. As a side effect of the V_O accumulation, we observe that the polaronic tail of the MES quasiparticle peak [18] notably reduces its spectral weight under irradiation due to increase of the MES concentration that screens the electron-phonon interaction.

The Ti^{3+}, IGS and MES_{xy}/MES_{yz} spectral weights, evaluated from the data in Fig. 2, are presented in Fig. 3(a) as a function of t_{irr}. To separate the IGS spectral contribution from the overlapping MES, we have averaged the ARPES intensity over the angular intervals outside the MES. The difference of these out-of-MES spectra from the zero-t_{irr} one, where the IGS-signal was negligible, identified the IGS spectra for every t_{irr}. The IGS weight W_{IGS} was then obtained by integration over the energy width of the IGS peak. To separate the MES contribution, in turn, we have averaged the ARPES intensity

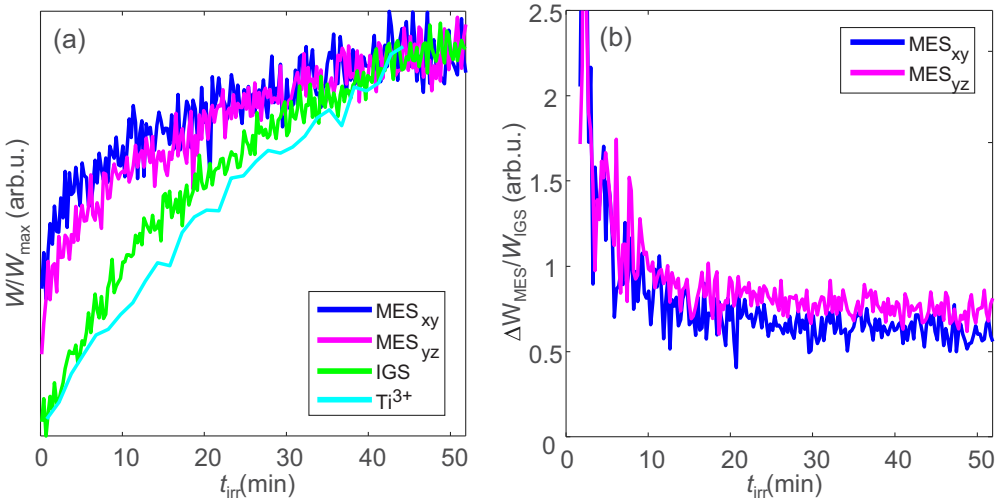

FIG. 3. (a) Ti^{3+}, IGS, and MES spectral weights, normalized to their maximal value, as a function of irradiation time; (b) The MES-to-IGS buildup ratio. The faster saturation of the MES signal compared to the IGS one indicates that at large V_O concentration the doped electrons preferentially populate the IGSs.

over the angular interval inside the MES and subtracted the corresponding out-of-MES spectra. The MES weight W_{MES} was determined by integration over the whole MES bandwidth including the polaronic tail. The two MES curves in Fig. 3(a) correspond to the two $h\nu$ values that boost the contribution of either d_{xy} or d_{yz} states in the total ARPES response. All curves are normalized here to their (statistically significant) value at maximal t_{irr}.

The t_{irr} dependences in Fig. 3(a) bear two important facts: (1) In the zero-t_{irr} limit, W_{MES} at both resonances extrapolates to certain nonzero value. In other words, the LAO/STO interface is conductive already without the V_Os. This fact supports the electrostatic scenarios of the LAO/STO conductivity as resulting from a redistribution of electrons to the interface to minimize the electrostatic energy created by polar discontinuity between LAO and STO. In these scenarios the MES electrons are injected by either states from the VB maximum of LAO pushed above E_F (the well-known "polar catastrophe") or from localized defect states in LAO created, for example, again by V_Os, which existed there before irradiation [21,38,45]; (2) As we have already mentioned, in a simplistic picture, one of the two electrons doped by each V_O localizes at the IGS, and another joins the mobile MES. Fig. 3(a) shows that whereas after ∼10 min of irradiation the production of both IGS and MES electrons slows down towards saturation, but for the MES the slowdown is stronger. This trend is emphasized in Fig. 3(b) as a ratio of the W_{MES} buildup ΔW_{MES} (relative to the zero-t_{irr} weight I_0) to W_{IGS}. This ratio dramatically drops towards $t_{irr} \sim 10$ min, indicating that at large V_O concentration the doped electrons tend to localize in the IGSs rather than escape into the MES. This observation still has to be fully understood, although a few theoretical works have demonstrated that properties of the V_Os depend on their concentration regime [21,46]. An ARPES study of the EPS at the bare STO(100) and (111) surfaces [16,28] has presented evidence that this phenomenon is driven by clustering of V_Os. Indeed, local-density approximation (LDA) $+U$ calculations on bare STO surfaces [21,46] suggest that the electron distribution between the MES and IGSs may depend on particular configurations of V_Os; while isolated V_Os on the surface tend to donate both released electrons into the MES, their cluster configurations favor even distribution. We note that the intensity evolution of the ARPES spectral structures under x-ray irradiation is accompanied by their energy shifts (see Supplemental Material 1 [35]).

B. Identification of EPS

We will now turn to the x-ray irradiation dynamics of **k**-resolved electron dispersions $E(\mathbf{k})$ and Fermi surface (FS). The progressive increase of the MES spectral intensity with irradiation, seen in Figs. 2(c) and 2(d) and quantified by W_{MES} in Fig. 3(a), evidences increase of the total concentration n_s^{tot} of the MES electrons. The first idea might be that this is caused by a progressive increase of the band population. The experimental **k**-resolved ARPES images acquired at small and large t_{irr} are displayed in Figs. 4(a) and 4(b). We observe, surprisingly, that these images demonstrate identical dispersions and population of the light d_{xy} and heavy d_{yz} bands, with the only difference being a rigid increase of their spectral intensity

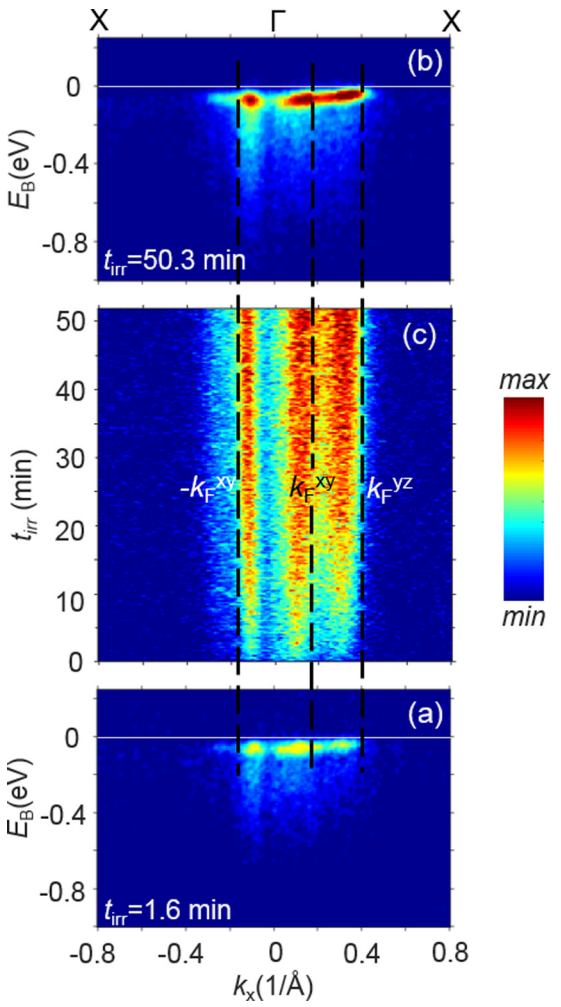

FIG. 4. Irradiation dependence of **k**-resolved electronic structure: (a),(b) ARPES images of $E(\mathbf{k})$ at small and large t_{irr} (indicated). (c) Fermi intensity as a function of t_{irr}. The k_F values corresponding to the d_{xy} and d_{yz} bands are marked through with dashed lines ($-k_F^{yz}$ is not visible because of the vanishing matrix element). The spectral intensity increase at constant band structure and k_F manifests the EPS.

(slight differences in the polaronic tale are beyond the scope of this work). The same behavior can be seen in ARPES data taken in other **k**-space regions (see Supplemental Material 2 [35]).

Furthermore, we have quantified k_F of the experimental bands as corresponding to maxima of the $-dI_F/d|k|$ negative gradient of the Fermi intensity. This method [47] is particularly suited for our case, where the bandwidth is comparable with the energy resolution, and the spectral intensity is significantly distorted by matrix-element variations. We find, remarkably, that the small- and large-t_{irr} ARPES images in Figs. 4(a) and 4(b) show identical $k_F \sim 0.4$ Å^{-1} (marked by dashed lines) even for the flat d_{yz} band most sensitive to its population. This fact identifies the same Luttinger counts n_s^{Lutt} of the FS embedding the MES electrons. Extending this observation, Fig. 4(c) shows a map of I_F through the whole range of t_{irr}. The k_F values determined by the gradient method (dashed lines, for the corresponding $-dI_F/d|k|$ map see

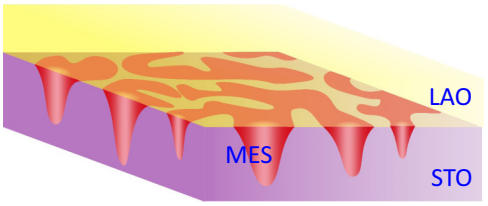

FIG. 5. Schematic representation of quasi-3D conducting puddles of MES in OD-LAO/STO.

Supplemental 2) are again constant, identifying constant n_s^{Lutt} for both d_{xy} and d_{yz} bands. The statistics of our experimental I_F and $-dI_F/d|k|$ maps shows this trend undoubtedly through the whole range of t_{irr} except perhaps k_F of the d_{yz} band in the region of very small t_{irr} where the ARPES signal is yet small.

The observed discrepancy between the total n_s^{tot}, increasing with t_{irr}, and constant n_s^{Lutt} can be reconciled within the EPS picture, where conducting puddles at the interface coexist with insulating ones. The MES signal in the ARPES spectra comes only from the conductive puddles, while the nonconducting ones stay silent. Upon x-ray irradiation and concomitant increase of the V_O concentration, the conducting puddles inflate their total interfacial fraction, as evidenced by scaling up of n_s^{tot}, whereas their local electronic structure stays the same as evidenced by their constant band structure and n_s^{Lutt} seen in ARPES. Due to the EPS, n_s^{Lutt} always promises larger n_s^{tot} than will actually be seen in electron transport. A sketch of the EPS in OD-LAO/STO, where the MES puddles have a quasi-3D character, is shown in Fig. 5.

The depth extension of MES in the OD-LAO/STO samples [20,21,48] is much more than $\lambda \sim 11$ Å at our kinetic energy [38,44]. Therefore, the observed ARPES intensity is roughly proportional to the lateral fraction of the conducting puddles, which we will call the lateral conducting fraction (LCF). In our case, the irradiation dynamics of the MES signal in Fig. 3(a) shows that from small to large t_{irr} the LCF increases by a factor ~3.3. As the LCF by definition cannot exceed 100%, we obtain its upper limit back to small oxygen deficiency as ~30%. An alternative way to assess the EPS, which is based on the MES intensity comparison to the Ti $2p$ peak, yields a similar estimate of the LCF (see Supplemental Material 3 [35]).

We note that the observed constant band structure parameters of the MES suggest that it has the same quasi-3D character already in the fresh samples. Indeed, the detection limit of our SX-ARPES experiment of ~1% corresponds to a spatial separation of the V_Os of ~40 Å, which is well within the overlap distance of the MES wave functions of about 60 Å [21]. Therefore, the spatial extension and thus dimensionality of the MES settle already at minute concentrations of V_Os.

C. Clustering of V_Os and its role in EPS

The parallel development of the IGS and MES signals with irradiation, observed in our experiments, suggests that the V_Os play an important role in the EPS. Indeed, theoretical analysis of interplay between the t_{2g} states of the MES with the orbitally reconstructed e_g states formed by the V_Os yields a rich phase diagram that includes regions of phase-separated

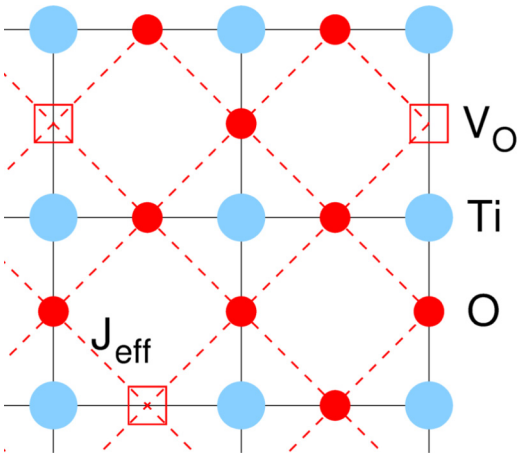

FIG. 6. Interface square lattice of oxygen ions in LAO/STO used in the J_{eff} analysis. A negative J_{eff} value favors clustering of V_Os.

magnetic states [25]. Furthermore, previous theoretical works predicted a tendency of V_Os to form clusters [49,50] which should unavoidably affect the EPS.

Our experimental data cannot directly elucidate the V_O-clustering tendency at the OD-LAO/STO interfaces. However, we can approach it via basic arguments from the alloy theory. Its cluster-expansion formalism provides a versatile tool to map lattice-configurational energies onto effective (Ising-like) interactions also for vacancy problems [51,52]. Here, we have employed density functional theory (DFT) as well as DFT plus dynamical-mean field theory (DFT+DMFT) – see Ref. [29] for particular computational details – to determine the respective configurational energies for a LAO/STO supercell. Based on these calculations, we have performed the binary-alloy mapping in the simplest nearest-neighbor pair approximation within an interface square lattice of oxygen ions (Fig. 6) where the site A was set to the O atom and B to the V_O. This picture yields an effective interaction integral $J_{eff} = \frac{1}{4}(E_{AA} - 2E_{AB} + E_{BB})$, where E_{AA} stands for the stoichiometric supercell energy, E_{AB} for the supercell with one V_O, and E_{BB} for the one with a nearest-neighbor double V_Os. Just as in the Ising theory of ordered magnetism, a positive J_{eff} drives alloy ordering ("antiferromagnetism"), while a negative one drives phase separation ("ferromagnetism"). Indeed, our calculations have revealed that in the LAO/STO case the effective pair interaction turns out negative, i.e., $J_{eff} = -143$ meV in the DFT framework and -155 meV in DFT+DMFT. Although a more thorough inclusion of further long-range interactions is needed for an accurate description of the defect interactions, this simple approximation already provides a good clue for a basic tendency towards clustering of V_Os in OD-LAO/STO. Our theoretical picture supports the conjecture of Li *et al.* [10] that the inhomogeneous distribution of V_Os stabilizes the magnetic order at the interface. On the experimental side, our irradiation-dependent PEEM measurements have shown that the size of the V_O clusters does not exceed 500 Å (see Supplemental Material 4 [35]).

The next important question on the physics of EPS that our experimental data cannot directly address is how are the MES puddles located relative to the V_O clusters? One can,

however, approach this question theoretically by considering which Ti 3*d* orbitals are involved in the MES vs V_O regions. Once the V_O clustering sets in, the orbitals mainly occupied in the V_O regions are the strongly localized Ti e_g ones, whereas in the fairly defect-free MES regions these orbitals are empty and only the strongly itinerant Ti t_{2g} orbitals are slightly occupied. Therefore, the MES tends to spatially separate from the V_O clusters. Surely, as it was shown recently [29], there is still a coupling between both orbital degrees of freedom, yet in main terms, the spatial separation of the MES from the V_Os via the distinct orbital characteristics carries over the V_O clustering into the electronic domain.

The formation of V_O clusters is also important for the magnetism of LAO/STO. Recent computational analysis including many-body correlations [23,24] suggest that already single-V_O configurations can build up the FM order. As observed in a theoretical study of the oxygen-deficient STO surface [27], the V_O clustering can promote, furthermore, a FM arrangement of the local moments originating from the nearby Ti sites.

D. EPS in ST-LAO/STO and discussion

How does the irradiation-tuned EPS observed at the OD-LAO/STO interfaces relate to the ST-ones? Because of the different MES dimensionality, the present results cannot be directly extrapolated to ST-LAO/STO. In that case, however, we can approach the intrinsic EPS by comparing the FS seen in the ARPES experiment with transport data. The previous SX-ARPES studies on ST-LAO/STO [18,19,42] find the FS where, evaluated from the $dI_F/d|k|$ minima, k_F of the d_{xy}-derived circular sheet is $\sim 0.07\,\text{Å}^{-1}$, and those of the $d_{xz/yz}$-derived elliptical sheets are ~ 0.33 and $\sim 0.12\,\text{Å}^{-1}$ along the long and short axes, respectively. These values yield the Luttinger count $n_s^{\text{Lutt}} \sim 7 \times 10^{13}\, e/\text{cm}^2$ which, because of the neglect of the smaller FS sheets derived from the d_{xy} states in deeper STO layers, should be considered as the lower estimate. The difference of this figure from n_s between 4 and 6×10^{13} detected by Hall measurements [42] identifies a significant EPS with an upper limit of the LCF of the order of 70%. This identification is corroborated by previous DFT calculations fitted to the transport n_s which, missing the EPS, produced systematically lower band energies (to embed more electrons) compared to the SX-ARPES experiment [42]. Similar reduction of n_s seen in the Hall effect has been noticed in comparison with results of inline electron holography [53]. We note that the experimental Luttinger count, characterizing the MES regions, is by a factor of almost five smaller than $n_s = 3.3 \times 10^{14}\, e/\text{cm}^2$ corresponding to $0.5\, e/\text{u.c.}$ of the ideal "polar catastrophe" scenario.

Our spectroscopic results on the EPS at the OD-LAO/STO interfaces and their above extension to the ST ones are consistent with a number of previous reports. For bare STO surfaces, the EPS developing under x-ray irradiation has been identified in an angle-integrated photoemission study [16,28]. For the LAO/STO interfaces, our area-sensitive spectroscopic evidence of the EPS is complemented by local methods such as scanning tunneling microscopy/spectroscopy [54,55] and atomic force microscopy [15] as well as from transport and magnetic properties [6,9]. Furthermore, our experimental results demonstrate that not only the electron dispersions and band population but also the energy broadening of the spectral peaks are independent of the interfacial conducting fraction up to its saturation. This behavior suggests that the interface separation into the conducting and nonconducting areas is sharp, without any significant variation of electronic structure between different conducting puddles. This fact casts doubt on previous conjectures that the EPS could be associated with variation of the band population along the interface, see Ref. [9], for example. On the theoretical side, Scopigno *et al.* [6] suggested that the EPS in ST-LAO/STO results from a lateral confinement tendency of the MES to avoid a thermodynamically unstable state with negative compressibility. Other non-V_O scenarios invoked formation of a Jahn-Teller polaronic phase [56], Rashba spin-orbit coupling [57,58], and even superconducting pairing interaction [58].

V. SUMMARY AND OUTLOOK

In summary, we have demonstrated EPS at LAO/STO interfaces tunable through their oxygen deficiency. Our experiment used ResPES at the Ti 2*p* edge to follow the evolution of the interfacial electronic structure as a function of V_O concentration gradually developing under x-ray irradiation. The V_Os generated by x-ray build up a dichotomic electron system where weakly correlated and nonmagnetic delocalized MES electrons coexist with strongly correlated and magnetic localized IGS electrons. The observed irradiation dynamics of the OD-LAO/STO electronic structure identifies the EPS as accumulation of the MES electrons in quasi-3D conducting puddles with fixed electronic structure, which are embedded in the insulating phase. Our theoretical analysis shows that the V_Os, promoted by the magnetism of the IGS electrons, tend to form clusters, and the MES puddles tend to spatially separate from them. Our PEEM data sets the upper limit on the V_O-cluster size as <500 Å. The intricate physics of the EPS, involving the interplay of the MES and IGSs, require further theoretical and experimental efforts where various area-sensitive spectroscopies such as ARPES are combined with local probes such as scanning tunneling microscopy/spectroscopy. Tunability of the EPS through oxygen deficiency can be used, on one end, for manipulation of electron transport properties of forthcoming oxide-based devices and, on the other end, their magnetic functionality. In this case the device heterostructures can be patterned using x-ray or e-beam lithography. The EPS persists intrinsically in the paradigm ST-LAO/STO case, with the upper limit of the LCF of the order of 70%.

The pronounced polaronic effects and the EPS are two native demerits of STO-based systems that fundamentally restrict, respectively, the mobility and concentration of charge carriers even under optimal tuning with oxygen deficiency. This fact calls for a search for other materials to replace STO as a standard platform for oxide electronics. The EPS can, however, be turned into an advantage of STO-based materials, where their natural separation into superconducting and ferromagnetic areas might allow an intrinsic realization of new device functionalities such as networks of ferromagnetic Josephson junctions.

ACKNOWLEDGMENTS

We thank R. Claessen, C. Cancellieri, M. Radovic, N. Pryds, U. Aschauer, G. Drera, and R. De Souza for sharing fruitful discussions. F.L. acknowledges financial support from the DFG Project No. LE 2446/4-1. DFT+DMFT computations were performed at the JUWELS Cluster of the Juelich Supercomputing Centre (JSC) under Project No. hhh08. A.C. and M.C. acknowledge funding from the Swiss National Science Foundation under Grant no. 200021_-165529.

[1] E. Dagotto, Science **309**, 257 (2005).

[2] V. B. Shenoy, D. D. Sarma, and C. N. R. Rao, ChemPhysChem **7**, 2053 (2006).

[3] V. B. Shenoy and C. N. R. Rao, Phil. Trans. R. Soc. A **366**, 63 (2008).

[4] J. Mannhart and D. G. Schlom, Science **327**, 1607 (2010).

[5] H. Y. Hwang, Y. Iwasa, M. Kawasaki, B. Keimer, N. Nagaosa, and Y. Tokura, Nature (London) Mater. **11**, 103 (2012).

[6] N. Scopigno, D. Bucheli, S. Caprara, J. Biscaras, N. Bergeal, J. Lesueur, and M. Grilli, Phys. Rev. Lett. **116**, 026804 (2016).

[7] S. Caprara, D. Bucheli, M. Grilli, J. Biscaras, N. Bergeal, S. Hurand, C. Feuillet-Palma, J. Lesueur, A. Rastogi, and R. C. Budhani, SPIN **04**, 1440004 (2014).

[8] D. Bucheli, S. Caprara, and M. Grilli, Supercond. Sci. Technol. **28**, 045004 (2015).

[9] Ariando, X. Wang, G. Baskaran, Z. Q. Liu, J. Huijben, J. B. Yi, A. Annadi, A. Roy Barman, A. Rusydi, S. Dhar, Y. P. Feng, J. Ding, H. Hilgenkamp, and T. Venkatesan, Nat. Commun. **2**, 188 (2011).

[10] L. Li, C. Richter, J. Mannhart, and R. C. Ashoori, Nat. Phys. **7**, 762 (2011).

[11] J. A. Bert, B. Kalisky, C. Bell, M. Kim, Y. Hikita, H. Y. Hwang, and K. A. Moler, Nat. Phys. **7**, 767 (2011).

[12] A. Joshua, J. Ruhman, S. Pecker, E. Altman, and S. Ilani, Proc. Natl. Acad. Sci. USA **110**, 9633 (2013).

[13] C. Richter, H. Boschker, W. Dietsche, E. Fillis-Tsirakis, R. Jany, F. Loder, L. F. Kourkoutis, D. A. Muller, J. R. Kirtley, C. W. Schneider, and J. Mannhart, Nature (London) **502**, 528 (2013).

[14] M. Coll, J. Fontcuberta, M. Althammer, M. Bibes, H. Boschker, A. Calleja, G. Cheng, M. Cuoco, R. Dittmann, B. Dkhil, I. El Baggari, M. Fanciulli, I. Fina, E. Fortunato, C. Frontera, S. Fujita, V. Garcia, S. T. B. Goennenwein, C. -G. Granqvist, J. Grollier, R. Gross, A. Hagfeldt, G. Herranz, K. Hono, E. Houwman, M. Huijben, A. Kalaboukhov, D. J. Keeble, G. Koster, L. F. Kourkoutis, J. Levy, M. Lira-Cantu, J. L. MacManus-Driscoll, J. Mannhart, R. Martins, S. Menzel, T. Mikolajick, M. Napari, M. D. Nguyen, G. Niklasson, C. Paillard, S. Panigrahi, G. Rijnders, F. Sánchez, P. Sanchis, S. Sanna, D. G. Schlom, U. Schroeder, K. M. Shen, A. Siemon, M. Spreitzer, H. Sukegawa, R. Tamayo, J. van den Brink, N. Pryds, and F. Miletto Granozio, Appl. Surf. Sci. **482**, 1 (2019).

[15] F. Bi, M. Huang, C.-W. Bark, S. Ryu, S. Lee, C.-B. Eom, P. Irvin, and J. Levy, J. Appl. Phys. **119**, 025309 (2016).

[16] L. Dudy, M. Sing, P. Scheiderer, J. D. Denlinger, P. Schütz, J. Gabel, M. Buchwald, C. Schlueter, T.-L. Lee, and R. Claessen, Adv. Mater. **28**, 7443 (2016).

[17] M. Altmeyer, H. O. Jeschke, O. Hijano-Cubelos, C. Martins, F. Lechermann, K. Koepernik, A. F. Santander-Syro, M. J. Rozenberg, R. Valentí, and M. Gabay, Phys. Rev. Lett. **116**, 157203 (2016).

[18] C. Cancellieri, A. S. Mishchenko, U. Aschauer, A. Filippetti, C. Faber, O. S. Barišić, V. A. Rogalev, T. Schmitt, N. Nagaosa, and V. N. Strocov, Nat. Commun. **7**, (2016).

[19] V. N. Strocov, C. Cancellieri, and A. S. Mishchenko, *Spectroscopy of Complex Oxide Interfaces* (Springer Series in Materials Science 266, 2018), p. 107.

[20] M. Basletic, J.-L. Maurice, C. Carrétéro, G. Herranz, O. Copie, M. Bibes, É. Jacquet, K. Bouzehouane, S. Fusil, and A. Barthélémy, Nat. Mater. **7**, 621 (2008).

[21] Y. Li, S. N. Phattalung, S. Limpijumnong, J. Kim, and J. Yu, Phys. Rev. B **84**, 245307 (2011).

[22] V. N. Strocov, M. Caputo, A. Chikina, M.-A. Husanu, L. L. Lev, C. Cancellieri, M. P. Mueller, M. Radovic, T. Schmitt, F. Miletto Granozio and R. A. De Souza, arxiv:1909.04106 (2019).

[23] F. Lechermann, L. Boehnke, D. Grieger, and C. Piefke, Phys. Rev. B **90**, 085125 (2014).

[24] M. Behrmann and F. Lechermann, Phys. Rev. B **92**, 125148 (2015).

[25] N. Pavlenko, T. Kopp, and J. Mannhart, Phys. Rev. B **88**, 201104(R) (2013).

[26] C. Lin and A. A. Demkov, Phys. Rev. Lett. **111**, 217601 (2013).

[27] F. Lechermann, H. O. Jeschke, A. J. Kim, S. Backes, and R. Valentí, Phys. Rev. B **93**, 121103(R) (2016).

[28] M. Sing, H. O. Jeschke, F. Lechermann, R. Valentí, and R. Claessen, Eur. Phys. J. Spec. Top. **226**, 2457 (2017).

[29] A. Chikina, F. Lechermann, M.-A. Husanu, M. Caputo, C. Cancellieri, X. Wang, T. Schmitt, M. Radovic, and V. N. Strocov, ACS Nano **12**, 7927 (2018).

[30] C. Cancellieri, N. Reyren, S. Gariglio, A. D. Caviglia, A. Fête, and J.-M. Triscone, EPL **91**, 17004 (2010).

[31] V. N. Strocov, L. L. Lev, M. Kobayashi, C. Cancellieri, M.-A. Husanu, A. Chikina, N. B. M. Schröter, X. Wang, J. A. Krieger, and Z. Salman, J. Electron Spectrosc. and Relat. Phenom. **236**, 1 (2019).

[32] V. N. Strocov, X. Wang, M. Shi, M. Kobayashi, J. Krempasky, C. Hess, T. Schmitt, and L. Patthey, J. Synchrotron Radiat. **21**, 32 (2014).

[33] V. N. Strocov, T. Schmitt, U. Flechsig, T. Schmidt, A. Imhof, Q. Chen, J. Raabe, R. Betemps, D. Zimoch, J. Krempasky, X. Wang, M. Grioni, A. Piazzalunga, and L. Patthey, J. Synchrotron Radiat. **17**, 631 (2010).

[34] J. Braun, J. Minár, S. Mankovsky, V. N. Strocov, N. B. Brookes, L. Plucinski, C. M. Schneider, C. S. Fadley, and H. Ebert, Phys. Rev. B **88**, 205409 (2013).

[35] See Supplemental Material at http://link.aps.org/supplemental/10.1103/PhysRevMaterials.3.106001 for further experimental results on x-ray irradiation dynamics including (1) Ti 2p core-level and valence-band energies, (2) band structure and Fermi surface in an extended **k**-space region, (3) LCF estimates based on the MES to Ti 2p signal ratio, and (4) results of microscopic studies with PEEM.

[36] U. Flechsig, F. Nolting, A. Fraile Rodríguez, J. Krempaský, C. Quitmann, T. Schmidt, S. Spielmann, D. Zimoch, R. Garrett, I. Gentle, K. Nugent, and S. Wilkins, AIP Conference Proceedings **1234**, 319 (2010).

[37] K. Szot, W. Speier, R. Carius, U. Zastrow, and W. Beyer, Phys. Rev. Lett. **88**, 075508 (2002).

[38] J. Gabel, M. Zapf, P. Scheiderer, P. Schütz, L. Dudy, M. Stübinger, C. Schlueter, T.-L. Lee, M. Sing, and R. Claessen, Phys. Rev. B **95**, 195109 (2017).

[39] Y. Z. Chen, M. Döbeli, E. Pomjakushina, Y. L. Gan, N. Pryds, and T. Lippert, Phys. Rev. Materials **1**, 052002(R) (2017).

[40] G. Berner, M. Sing, H. Fujiwara, A. Yasui, Y. Saitoh, A. Yamasaki, Y. Nishitani, A. Sekiyama, N. Pavlenko, T. Kopp, C. Richter, J. Mannhart, S. Suga, and R. Claessen, Phys. Rev. Lett. **110**, 247601 (2013).

[41] G. Drera, G. Salvinelli, F. Bondino, E. Magnano, M. Huijben, A. Brinkman, and L. Sangaletti, Phys. Rev. B **90**, 035124 (2014).

[42] C. Cancellieri, M. L. Reinle-Schmitt, M. Kobayashi, V. N. Strocov, P. R. Willmott, D. Fontaine, P. Ghosez, A. Filippetti, P. Delugas, and V. Fiorentini, Phys. Rev. B **89**, 121412(R) (2014).

[43] V. N. Strocov, J. Electron Spectrosc. Relat. Phenom. **229**, 100 (2018).

[44] C. J. Powell, A. Jablonski, S. Tanuma, and D. R. Penn, J. Electron Spectrosc. Relat. Phenom. **68**, 605 (1994).

[45] N. C. Bristowe, P. B. Littlewood, and E. Artacho, Phys. Rev. B **83**, 205405 (2011).

[46] H. O. Jeschke, J. Shen, and R. Valentí, New J. Phys. **17**, 023034 (2015).

[47] T. Straub, R. Claessen, P. Steiner, S. Hüfner, V. Eyert, K. Friemelt, and E. Bucher, Phys. Rev. B **55**, 13473 (1997).

[48] S. Gariglio, A. Fête, and J.-M. Triscone, J. Phys. Condens. Matter **27**, 283201 (2015).

[49] N. Pavlenko, T. Kopp, E. Y. Tsymbal, G. A. Sawatzky, and J. Mannhart, Phys. Rev. B **85**, 020407(R) (2012).

[50] N. Mohanta and A. Taraphder, J. Phys. Condens. Matter **26**, 215703 (2014).

[51] F. Lechermann and M. Fähnle, Phys. Rev. B **63**, 012104 (2000).

[52] P. A. Korzhavyi, C. Ambrosch-Draxl, and B. Johansson, J. Low Temp. Phys. **117**, 395 (1999).

[53] K. Song, S. Ryu, H. Lee, T. R. Paudel, C. T. Koch, B. Park, J. K. Lee, S.-Y. Choi, Y.-M. Kim, J. C. Kim, H. Y. Jeong, M. S. Rzchowski, E. Y. Tsymbal, C.-B. Eom, and S. H. Oh, Nat. Nanotechnol. **13**, 198 (2018).

[54] M. Breitschaft, V. Tinkl, N. Pavlenko, S. Paetel, C. Richter, J. R. Kirtley, Y. C. Liao, G. Hammerl, V. Eyert, T. Kopp, and J. Mannhart, Phys. Rev. B **81**, 153414 (2010).

[55] Z. Ristic, R. Di Capua, G. M. De Luca, F. Chiarella, G. Ghiringhelli, J. C. Cezar, N. B. Brookes, C. Richter, J. Mannhart, and M. Salluzzo, EPL **93**, 17004 (2011).

[56] B. R. K. Nanda and S. Satpathy, Phys. Rev. B **83**, 195114 (2011).

[57] G. Seibold, S. Caprara, M. Grilli, and R. Raimondi, EPL **112**, 17004 (2015).

[58] N. Bovenzi, F. Finocchiaro, N. Scopigno, D. Bucheli, S. Caprara, G. Seibold, and M. Grilli, J. Supercond. Novel Magn. **28**, 1273 (2015).